SCANNING VOL. 34, 316–324 (2012)

AFM Feature Definition for Neural Cells on Nanofibrillar Tissue Scaffolds

Volkan M. Tiryaki[1], Adeel A. Khan[2], and Virginia M. Ayres[1]

[1]Department of Electrical and Computer Engineering, Michigan State University, East Lansing, Michigan
[2]Department of Paper Engineering, Chemical Engineering and Imaging, Western Michigan University, Kalamazoo, Michigan

Summary: A diagnostic approach is developed and implemented that provides clear feature definition in atomic force microscopy (AFM) images of neural cells on nanofibrillar tissue scaffolds. Because the cellular edges and processes are on the same order as the background nanofibers, this imaging situation presents a feature definition problem. The diagnostic approach is based on analysis of discrete Fourier transforms of standard AFM section measurements. The diagnostic conclusion that the combination of dynamic range enhancement with low-frequency component suppression enhances feature definition is shown to be correct and to lead to clear-featured images that could change previously held assumptions about the cell–cell interactions present. Clear feature definition of cells on scaffolds extends the usefulness of AFM imaging for use in regenerative medicine. SCANNING 34: 316–324, 2012. © 2012 Wiley Periodicals, Inc.

Key words: AFM/other scanned probe microscopies, image processing, image analysis, life sciences

Contract grant sponsor: National Science Foundation, Contract grant number: PHY-0957776; Contract grant sponsor: General Directorate for Higher Education, Ministry of National Education of the Republic of Turkey; Contract grant sponsor: Michigan-Louis Stokes Alliance for Minority Participation Summer Undergraduate Research Academy.

Address for reprints: Volkan M. Tiryaki, Department of Electrical and Computer Engineering, Room 2120 Engineering Building, Michigan State University, East Lansing, MI 48824. E-mail: tiryakiv@msu.edu

Received 4 November 2011; Accepted with revision 23 December 2011

DOI 10.1002/sca.21013
Published online 14 May 2012 in Wiley Online Library (wileyonlinelibrary.com)

Introduction

The use of atomic force microscopy (AFM) in biomedical investigation has grown rapidly, with recent exciting applications in diverse fields including regenerative medicine (tissue engineering) (Fan *et al.*, 2007; Tiryaki *et al.*, 2010), drug delivery (Sitterberg *et al.*, 2010), protein folding (Wang *et al.*, 2011), and clinical medicine (Kreplak *et al.*, 2007). Even so, AFM remains an underutilized technique within the biomedical research community and more importantly an underdeveloped enabler of significant new nanoscale biomedical discoveries due to a general problem with inconsistent feature definition. When a feature definition problem is encountered, the standard approach is to use instrument-supplied hardware or software capabilities to resolve it. Deflection imaging (contact mode) or phase imaging (tapping mode) can improve feature definition when changes in cantilever deflection or RMS cantilever oscillation are greatest at boundaries. Alternatively, image processing can be used to extract information that actually exists in an AFM image but is inaccessible prior to processing. Useful filters are a standard component of commercial image processing packages for AFMs, and low-pass filtering for noise reduction is a known and popular approach. However, for either hardware or software approaches to be successful, it is key to diagnose and accurately identify the nature of the feature definition problem involved. As will be shown, low-pass filtering can be the wrong approach to improve feature definition. There has been comparatively little systematic methodology developed for image diagnosis, other than user experience. This can make the AFM learning curve a lengthy one for new biomedical researchers, especially for certain classes of biomedical problems that have feature definition issues.

In the present work, a severe problem with feature definition of astrocyte neural cells on a promising prosthetic nanofibrillar scaffold for brain and spinal cord injury repair (Meiners *et al.*, 2007; Meiners

et al., 2009) is first diagnosed and then resolved. Recent studies indicate that cells grown on nanofibrillar surfaces that approximate their native extracellular matrix (ECM) environments behave differently, and in seemingly more biomimetic ways (Georges *et al.*, 2006; Delgado-Rivera *et al.*, 2009). Many details of the cell–cell and cell–scaffold interactions that may induce the biomimetic response are not presently well known. This is therefore a research area in which the nanoscale resolution capability of AFM could offer significant biomedical insights. The difficulty with AFM investigation is that cells on nanofibrillar surfaces interact with these surfaces via nanoscale edges and processes that are not distinguishable from the nanofibrillar background by height, deflection, or phase imaging. This is because the cellular edges and processes are approximately the same order in height as the background nanofibers, ~100 to 200 nm. We demonstrate that this problem can be resolved by filtering and present a novel diagnostic approach based on standard AFM section measurements to enable knowledgeable filter selection and design. The requirements for successful image processing were identified as a combination of low-frequency component suppression with dynamic range enhancement. This design was implemented to filter the harmonic components present in the images in such a way that the cellular edges and processes became distinguishable from the nanofibrillar backgrounds. We demonstrate that the new information revealed in the filtered AFM images would change the biomedical interpretations drawn about the cell–cell interactions present, especially when compared with a more typical analysis of fluorescent microscopy images.

Material and Methods

Neural Cell Culture

Rat cerebral cortical astrocytes were prepared from postnatal day 1 (P1) Sprague Dawley rats and grown to confluence in astrocyte medium in 75-cm^2 tissue culture flasks as previously described (Delgado-Rivera *et al.*, 2009). The astrocyte culture medium was comprised of Dulbecco's Modified Eagle's Medium (Invitrogen, Carlsbad, CA) +10% calf serum (Invitrogen). After reaching confluence (~8–10 days), flasks were shaken overnight on a rotary shaker at 37 °C to remove any loosely adherent oligodendrocytes, neurons, or macrophages. Astrocytes were then subcultured in astrocyte medium (0.5 ml) at a density of 50,000 cells/well onto 12-mm coverslips coated with nanofibers in 24-well trays. The astrocytes were maintained for 24 h. The astrocytes were then fixed with paraformaldehyde (4%) and stained with phalloidin (Schindler *et al.*, 2005) for fluorescent microscopy investigation. Staining did not affect the AFM imaging.

Nanofibrillar Culture Surface

Randomly oriented polyamide nanofibers (median diameter ~180 nm) were electrospun from a blend (Chung *et al.*, 2004; Schindler *et al.*, 2005) of two polymers [$(C_{28}O_4N_4H_{47})_n$ and $(C_{27}O_{4.4}N_4H_{50})_n$] onto plastic ACLAR coverslips (Ted Pella, Reading, CA) by Donaldson Co., Inc. (Minneapolis, MN). Crosslinking of nanofibers was done in the presence of an acid catalyst. The resulting nonwoven polymeric nanofibrillar matrix was approximately 2.0-μm thick when measured on edge by optical microscopy, with no direct openings to the coverslip surface (Grafe and Graham, 2002; Ahmed *et al.*, 2006).

Epi-Fluorescence Microscopy

Epi-fluorescence microscopy images of astrocyte neural cell cultures at 24 h were captured using a Zeiss Axioplan microscope (Carl Zeiss Microimaging GmbH, Jena, Germany). Fluorescence optical microscopy is the most widely utilized technique for cell culture analysis.

Atomic Force Microscopy (AFM)

AFM images of astrocyte neural cell cultures at 24 h were captured using a Nanoscope IIIA (Bruker AXS Inc, Madison WI, formerly Veeco Metrology) operated in ambient air. Wide-area images showing cell groups were acquired using a J scanner with a maximum scan range of 125 × 125 μm^2 x–y range and ±2.774 μm z range with the AFM was operated in contact mode, using silicon nitride tips with a nominal tip radius of 20 nm and a cantilever spring constant $k = 0.58$ N/m. Close-up images of cell-scaffold interactions were acquired using an E scanner with a maximum scan range of 13.5 × 13.5 μm^2 x–y range and ±1.54 μm z range with the AFM was operated in tapping mode, using etched silicon tips with a nominal tip radius of 10 nm and a drive frequency of ~320 kHz.

Image Processing Methods

Digital image processing techniques were implemented with MATLAB version 7.6.0 (R2008a) (The MathWorks, Natic, MA). Digital images were exported as ASCII files from the Nanoscope Software version 5.30r3.sr3 by converting the units to nanometer. Four different types of two-dimensional finite

impulse response digital filters were evaluated in this work: frequency domain Gaussian and Butterworth high-pass filters, spatial domain high-pass filters, and high-boost filters. The Gaussian and Butterworth high-pass filters were implemented over frequency domain with normalized cutoff frequencies (ω/π) from 0 to 1 and with integer degrees from 1 to 5. As a final step, histogram equalization was applied for contrast enhancement (MATLAB®).

Gaussian High-Pass Filter (GHPF) Implementation

Image enhancement in the frequency domain is based on the computation of the two-dimensional discrete Fourier transform (DFT) of the input image, followed by multiplication of the result by a filter transfer function. The final output is obtained by taking the inverse two-dimensional DFT of the product. The fast Fourier transform, the computationally efficient algorithm (Frigo and Johnson, '98) for computing DFT, was performed for all of the DFT computations throughout this work.

The two-dimensional DFT of an $M \times N$ pixel image was calculated as

$$F(u, v) = \frac{1}{MN} \sum_{x=0}^{M-1} \sum_{y=0}^{N-1} f(x, y) \times \exp\left[-j2\pi \left(\frac{ux}{M} + \frac{vy}{N}\right)\right], \quad (1)$$

where x and y are the spatial variables, $f(x,y)$ is the raw image, u and v are the frequency domain variables, and F is the two-dimensional DFT of the $M \times N$ pixel image.

The GHPF transfer function was implemented as

$$H(u, v) = 1 - \exp\left[-\frac{D(u, v)^2}{2D_0^2}\right], \quad (2)$$

where D_0 is the cutoff frequency and $D(u,v)$ is the distance from (u,v) to the origin. To apply the GHPF to the image, $F(u,v)$ and $H(u,v)$ were multiplied by array multiplication. $G(u,v) = F(u,v)H(u,v)$ and the inverse two-dimensional DFT defined as

$$g(x, y) = \sum_{u=0}^{M-1} \sum_{v=0}^{N-1} G(u, v) \exp\left[j2\pi \left(\frac{ux}{M} + \frac{vy}{N}\right)\right] \quad (3)$$

was applied, and the final GHPF result was obtained.

High-Boost Filtering Implementation

High-boost, or high-frequency emphasis, filtering is based on adding a specified percent of the original image to the high-pass filtered image (Gonzalez and Woods, 2008). This addition restores the low-frequency components that were lost in the high-pass filtering operation, so the resulting image may look more like the original image. This was attractive for reinclusion of cell surface features. A high-boost filter was implemented as

$$Y = (A - 1)O + H, \quad (4)$$

where Y is the filter output, A is the amplification factor, O is the original image, and H is the high-pass filtered image.

Histogram Equalization for Contrast Enhancement

A histogram equalization was performed in order to enhance the contrast of the filtered images. The image contrasts were enhanced by transforming the values in the filtered image, so that the histogram of the output image had a roughly equal number of pixels mapped to each of its 256 levels. The histogram equalization operation converted the low-contrast and dark images to relatively higher contrast and brighter images.

Results

In this section, we first identify the feature definition problem found in distinguishing thin neural cell processes and edges from the tissue-culture surfaces that have nanoscale features. Our quantitative problem diagnosis procedure is presented next. The optimal filter design based on the problem diagnosis is then given, and finally, the biomedical interpretations drawn from analyzing images with missing versus complete information are discussed.

Feature Definition Problem

A composite AFM height image of a three-astrocyte group on a nanofibrillar surface is shown in Figure 1(a). The feature definition is poor for both the cell edges and the cellular processes (extensions with which a cell explores its environment). The structures marked by arrows in the AFM height image of Figure 1(a) could be either nanofibers or cellular processes. Close-ups of potentially important cell–scaffold interactions (dashed box in Fig. 1(a)) were investigated by AFM tapping mode phase images. As shown in Figure 1(b), this did not improve the feature definition. The problem is that the cellular edges and processes are approximately the same order in height as the background nanofibers, ~100 to 200 nm.

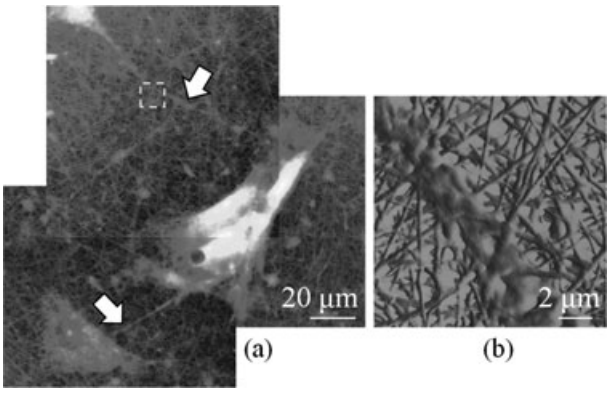

Fig 1. Feature definition problems of astrocyte neural cells on nanofibrillar surfaces. (a) The structures marked by arrows in the AFM height image could be either nanofibers or processes. (b) A higher resolution closeup tapping mode phase image of the region shown by dashed box in (a). Its edge features are still unclear.

Systematic Approach to Problem Diagnosis

A diagnostic approach based on standard AFM section measurements was developed. Individual section measurements of the nanofibrillar surface and an astrocyte cell body are shown in Figure 2(a)/(b) and (d)/(e). A one-dimensional DFT was then applied to the section measurement data of Figure 2(b) and (e). This converted the section measurements into the frequency domain where the harmonic components could be studied and analyzed. The magnitudes of the DFT spectra were then calculated, and the logarithmic DFT spectra were plotted. The logarithmic DFT spectra shown in Figure 2(c) and (f) can be used to identify the key differences between the cell and nanofibrillar surfaces, which can then be used to create an optimal filter design. In the present case, the differences were

1. The one-dimensional DFT spectra in Figure 2(c) and (f) demonstrated that the amplitude of the zero-frequency sample of the cell profile was approximately fivefold higher than the amplitude of the zero frequency of the nanofibrillar profile. This suggested that attenuation of the zero-frequency sample and the other low-frequency components with a high-pass filter would result in deemphasizing the astrocyte surface relative to the nanofibers so that the astrocyte surface could be distinguished from the nanofibrillar background. This is known as dynamic range enhancement.
2. The nanofibrillar surface had sharper features, meaning more power in the higher frequency harmonics than the astrocyte surface. The high-frequency harmonic region above cutoff frequency 0.5 (red dotted lines) had 52% more power than the same frequency region for the astrocyte DFT spectrum.
3. The low-frequency harmonics of astrocytes and nanofibers were overlapping in the DFT spectra (Fig. 2(c) and (f)). Therefore, total elimination of cell surface information while retaining the nanofibrillar surface information is not possible by filtering techniques. However, because the high-frequency components of nanofibrillar surface had more power than the high-frequency components of astrocyte surfaces, as shown in Figure 2(c) and (f), amplification of the high-frequency components would exaggerate the difference between nanofibers and astrocytes. This is achieved

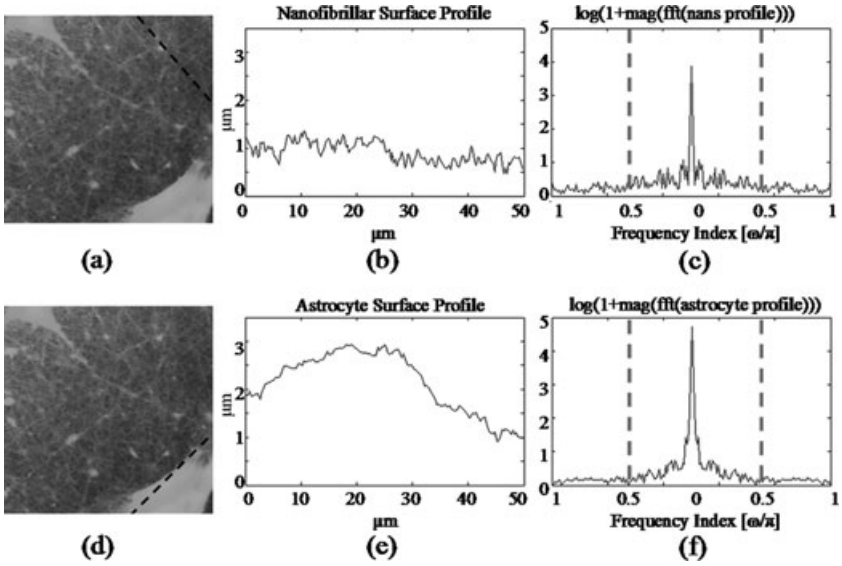

Fig 2. (a) Section measurement of nanofibrillar surface along dashed line, (b) corresponding surface profile, and (c) DFT of nanofibrillar surface profile. (d) Section measurement of cell surface along dashed line (e) corresponding surface profile, and (f) DFT of cell surface profile.

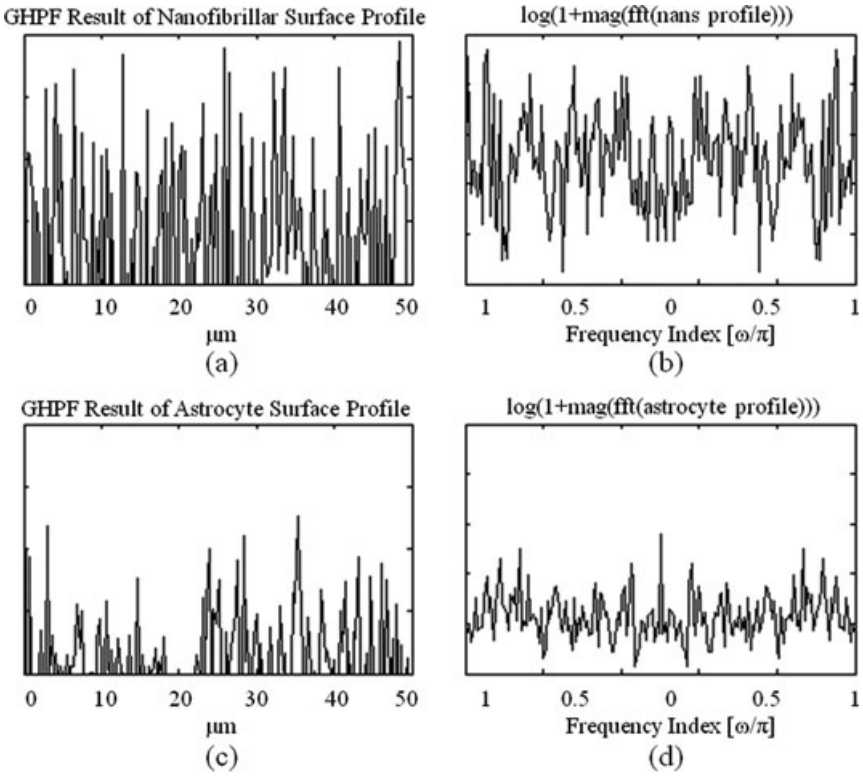

Fig 3. GHPF results (a) filtered nanofibrillar surface profile, (b) DFT spectrum of the nanofibrillar surface profile, (c) filtered astrocyte surface profile, and (d) DFT spectrum of the astrocyte surface profile.

by using a high-pass, not a low-pass, filter. The results of a preliminary test using a GHPF, shown in space and *k*-space domains in Figure 3, confirmed this approach. When the GHPF surface profiles shown in Figure 3(a) and (c) are compared, we see that the nanofibrillar surface has higher edge features than the astrocytes. Figure 3(b) and (d) show that the high-frequency harmonics of nanofibrillar substrate has more power than the high-frequency harmonics of astrocyte surface. These quantitative differences are the basis for the subsequent successful filter design.

Optimal Filter Design Based on Problem Diagnosis

The Gaussian and Butterworth frequency domain high-pass filters were implemented by changing the order and the cutoff frequency of the filter. Optimum results were obtained with a GHPF transfer function of order 1 and normalized cutoff frequency 0.5. The perspective plot of the GHPF transfer function of order 1 and normalized cutoff frequency 0.5 is shown in Figure 4(a) and the radial cross section of the transfer function is shown in Figure 4(b). Figure 4(a) shows that the Gaussian frequency domain high-pass filter is positional invariant or isotropic. Application of the Butterworth filter yielded noisier results, therefore identifying the optimized GHPF as preferable.

Spatial domain filters were also investigated, both as an alternative to frequency domain filter and because of our interest in high-boost filtering, a variant of spatial filtering, for return of cell features to filtered images. Spatial domain filters require the specification of a mask. In the present work, 3×3, 5×5, and 7×7 spatial high-pass masks were investigated, and 3×3 mask size was identified as optimal. High-boost filtering was therefore performed using a 3×3 spatial high-pass mask. Amplification factors of 1.05, 1.10, 1.15, and 1.20 were implemented, and 1.15 was optimum. However, the high-boost filtering technique was not successful in our case because return of the 15% of the original image also compressed the dynamic range to the point where cellular edge and process feature definitions were unacceptably reduced. Furthermore, analysis of spatial domain transfer functions (not shown) revealed positional anisotropy that would introduce distortions into filtered images of randomly oriented nanofibers. These investigations enabled the systematic selection of the GHPF as best for our investigations.

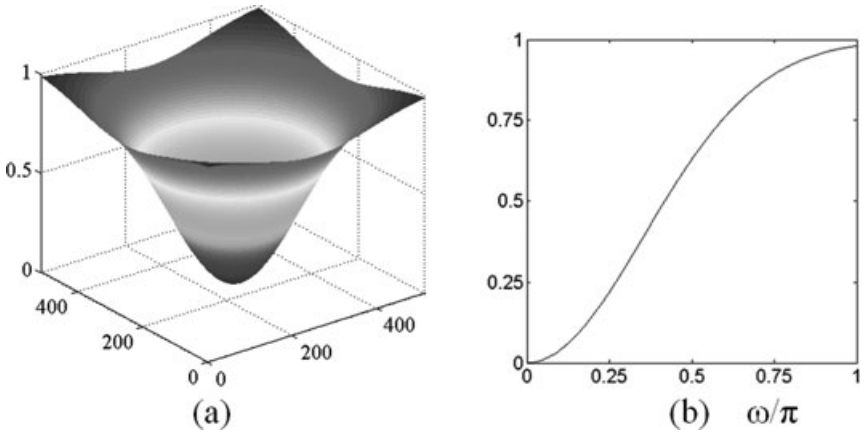

Fig 4. (a) Perspective plot and (b) radial cross section of the GHPF transfer function of order 1 and normalized cutoff frequency 0.5. The zero frequency sample is at the center in (a).

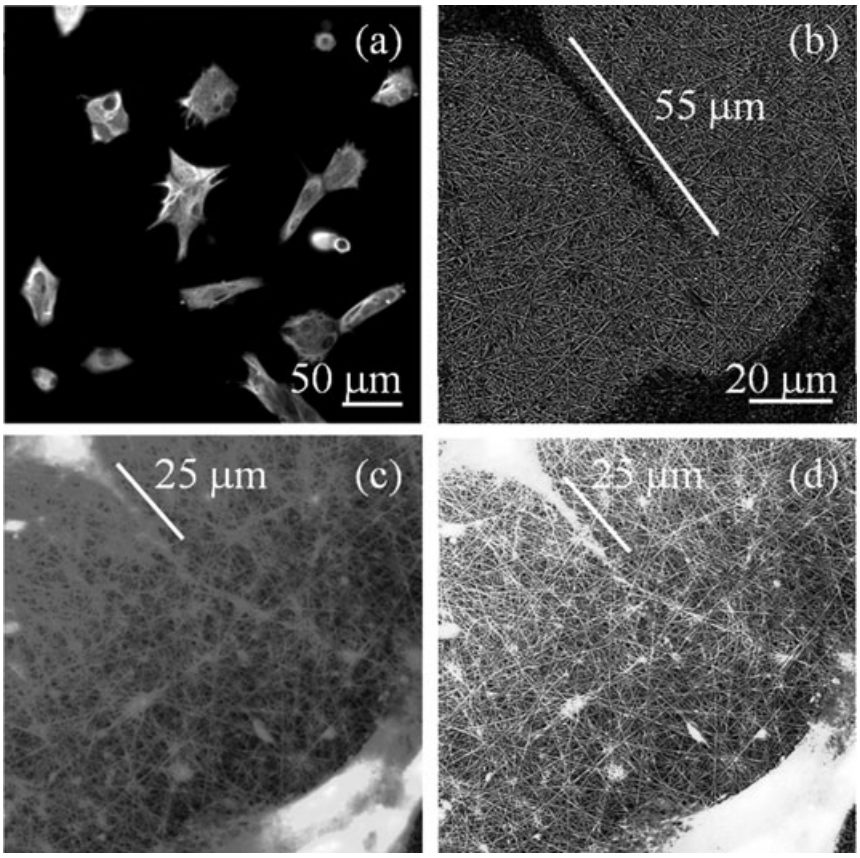

Fig 5. (a) Epi-fluorescence microscopy image of "isolated" astrocytes at 24 h. (b) GHPF AFM image revealed significant leading edge formation. (c) Unfiltered AFM image did not show full extent of leading edge formation. (d) Inclusion of 15% of original image in high-boost filtering resulted in loss of feature definition to a level comparable to unfiltered AFM image.

Biomedical Interpretations Based on Fluorescence Microscopy, AFM, and GHPF AFM Height Images

Cell culture protocols include inspection for cell morphology at regular intervals, e.g., at 24 h and 48 h, typically performed using optical microscopy. In a coordinated epi-fluorescence microscopy/AFM investigation (Tiryaki *et al.*, 2011), a series of images from different regions of the astrocyte-on-scaffold cell cultures were acquired using epi-fluorescence microscopy. The epi-fluorescence microscopy images (Fig. 5(a)) indicated that the astrocytes were stellate but largely isolated from each other at 24 h. AFM height image of astrocytes cultured on nanofibrillar surfaces, shown in Figure 5(c), would not contradict the conclusion that the cells were stellate and largely

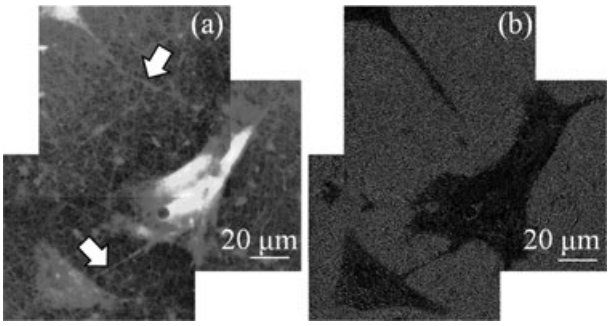

Fig 6. In the composite AFM height image (a), cellular processes and cell edges are indistinguishable from the nanofibrillar background. (b) In the GHPF result, the cellular edges and processes are clearly distinguished from nanofibrillar scaffold.

isolated at 24 h. However, the clear feature definition of cellular edges and processes obtained by application of the GHPF filter, shown in Figure 5(b), demonstrated that significant leading edge formation beyond the previously assumed process ending had occurred at 24 h. The high-boost filtering result shown in Figure 5(d) demonstrates that loss of dynamic range enhancement by inclusion of as little as 15% of the original image resulted in loss of feature definition to a level comparable to that of an unfiltered AFM image.

The unfiltered height image of Figure 1(a) is reproduced in Figure 6(a) and compared with its GHPF equivalent in Figure 6(b). In addition to the long process described in Figure 5, the filtered image revealed a second complete cellular bridge that extended between the "isolated" cells. Direct contact via cellular bridges has implications for intercellular information exchange (Gerdes and Carvalho, 2008) and, using the methods developed in this article, our group is the first to report this possibility for neural cells on nanofibrillar surfaces.

Discussion

In this work, DFTs of standard AFM section measurements of astrocytes versus nanofibrillar surfaces were used as the basis for the diagnosis of the feature definition problem. These showed that the high-frequency components of nanofibrillar surface had more power than the high-frequency components of astrocyte surfaces and identified the use of a frequency domain high-pass filter as the potential solution to the feature definition problem. Such a filter has two advantages. The high-frequency components of the nanofibrillar surface are amplified, making them easier to distinguish from the cellular features. Furthermore, suppression of the low-frequency components yields a dynamic range enhancement of the image. The diagnostic conclusions were therefore that the combination of dynamic range enhancement with low-frequency component suppression that could be achieved through frequency domain high-pass filtering would be likely to enhance feature definition of cellular edges and process relative to nanofibrillar tissue scaffolds. A GHPF filter of appropriate degree and cutoff frequency was designed and used to selectively emphasize the high-frequency harmonics that belonged to nanofibers of the tissue culture scaffold, enabling the nanoscale cellular edges and processes to be distinguished from nanofibrillar surfaces. We further demonstrated that the high-boost filtering technique, although attractive for inclusion of cell surface features, was not successful in our problem because the return of as little as 15% of the original image also compressed the dynamic range with unacceptable loss of cellular feature definition relative to the nanofibrillar surface. We note in passing that the information needed for clear feature definition was contained in the AFM images all along. The problem was not a damaged or dirty tip, or poor tracking.

The GHPF filter of the present study was successfully applied to more than 250 contact and tapping mode AFM height images of cerebral cortical astrocytes cultured on poly-L-lysine functionalized glass, nanofibrillar scaffolds, and fibroblast growth factor-2 derivatized nanofibers; and also cerebellar granular neurons cultured on nanofibrillar scaffolds and poly-L-lysine functionalized glass. While this suggests that the GHPF filter with selected degree and cutoff frequencies has general utility in cell culture investigations, the major emphasis of this study is on the simple diagnostic approach that identified it. The diagnosis and custom filter design approach presented here expands user options beyond the selection supplied with the instrument or toward more knowledgeable use of instrument supplied filters. It also enables the user to connect with the growing body of work in image enhancement methods for AFM images for biological samples (Kienberger *et al.*, 2006), for nonbiological samples (Liu *et al.*, 2010), and in general (Osher and Rudin, 90; Alvarez and Mazorra, 94; Gilboa *et al.*, 2002).

The electrospun polyamide nanofibrillar matrices of the present study have shown promising results for spinal cord repair (Meiners *et al.*, 2007; Meiners *et al.*, 2009). There are many other types of nanofibrillar prosthetics currently under investigation for different injury repair situations, including self-assembling peptide nanofibers (Zou *et al.*, 2010), porous hydrogels (Hwang *et al.*, 2010), self-assembling nanofibrous gels (Zhou *et al.*, 2009), and ECM allografts (Lisy *et al.*, 2010). Many potentially significant details of the cell–cell and cell–scaffold interactions are not presently known and the nanoscale resolution of AFM could offer significant biomedical insights. However, AFM investigation of cells on any of these surfaces would encounter the same problem described in the present work: that the dynamic range of the

captured images is insufficient to allow thin ~20–100 nm layers of cytoplasm to be distinguished from ~100 to 200 nm nanofeatured surfaces.

GHPF AFM height images revealed that these nanofibrillar surfaces enable the development of previously unknown astrocyte cell–cell interactions by 24 h, which provides new information for ongoing investigations of why cells cultured on nanofibrillar surfaces seem more biomimetic. The same techniques were successfully applied for cerebellar granular neurons cultured on nanofibrillar surfaces and should be useful in similar investigations, e.g., cardiomyocytes on nanofibrillar surfaces. The methods developed here can therefore extend the usefulness of AFM nanoscale imaging in regenerative medicine.

Conclusions

In this work, a diagnostic approach based on analysis of DFTs of standard AFM section measurements was developed and used to identify quantitative differences in the frequency components of nanoscale cellular edges and processes of neural cells cultured on nanofibrillar scaffolds. Accurate identification of differences formed the basis for the subsequent successful GHPF design that enabled the edges and processes to be clearly distinguished in AFM images. The samples are astrocyte neural cells cultured on nanofibrillar tissue scaffolds that have shown promise for spinal cord injury repair. The diagnostic approach presented here can enable more knowledgeable filter selection or design in any field and can extend the usefulness of AFM nanoscale imaging in the field of regenerative medicine.

Acknowledgement

The authors also gratefully acknowledge Dr. Ijaz Ahmed (Rutgers, The State University of New Jersey) for the astrocyte cell cultures and the epi-fluorescence microscopy investigation. Authors do not have conflict of interest to declare.

References

Ahmed I, Liu H-Y, Mamiya PC, Ponery AS, Babu AN, *et al.* 2006. Three-dimensional nanofibrillar surfaces covalently modified with tenascin-C-derived peptides enhance neuronal growth in vitro. J Biomed Mater Res A 76:851–860.

Alvarez L, Mazorra L. 1994. Signal and image retoration using shock filters and anisotropic diffusion. SIAM J Numer Anal 31:590–605.

Chung HY, Hal JRB, Gogins MA, Crofoot DG, Weik TM. 2004. Polymer, polymer microfiber, polymer nanofiber and applications including filter structures. US Patent No 6,743,273 B2.

Delgado-Rivera R, Harris SL, Ahmed I, Babu AN, Patel R, *et al.* 2009. Increased FGF-2 secretion and ability to support neurite outgrowth by astrocytes cultured on polyamide nanofibrillar matrices. Matrix Biol 28:137–147.

Fan Y, Chen Q, Ayres VM, Baczewski AD, Udpa L, *et al.* 2007. Scanning probe recognition microscopy investigation of tissue scaffold properties. Int J Nanomedicine 2:651–661.

Frigo M, Johnson SG. 1998. FFTW: an adaptive software architecture for the FFT. Proceedings of the International Conference on Acoustics, Speech, and Signal Processing 3:1381–1384.

Georges PC, Miller WJ, Meaney DF, Sawyer ES, Janmey PA. 2006. Matrices with compliance comparable to that of brain tissue select neuronal over glial growth in mixed cortical cultures. Biophys J 90:3012–3018.

Gerdes HH, Carvalho RN 2008. Intercellular transfer mediated by tunneling nanotubes. Curr Opin Cell Biol 20:474–475.

Gilboa G, Sochen N, Zeevi YY. 2002. Regularized shock filters and complex diffusion. Proceedings of the European Conference on Computer Vision'02:399–313.

Gonzalez RC, Woods RE. 2008. Digital Image Processing 3rd ed. Prentice Hall, Upper Saddle River, NJ .

Grafe T, Graham K. 2002. Polymeric nanofibers and nanofiber webs: a new class of nonwovens. Proceedings of the International Nonwovens Technical Conference, Atlanta, Georgia, September 24–26.

Hwang CM, Sant S, Masaeli M, Kachouie NN, Zamanian B, *et al.* 2010. Fabrication of three-dimensional porous cell-laden hydrogel for tissue engineering. Biofabrication 2:1–12.

Kienberger F, Pastushenko VP, Kada G, Puntheeranurak T, Chtcheglova L, *et al.* 2006. Improving the contrast of topographical AFM images by a simple averaging filter. Ultramicroscopy 106:822–828.

Kreplak L, Wang H, Aebi U, Kong X. 2007. Atomic force microscopy of mammalian urothelial surface. J Mol Biol 374:365–373.

Lisy M, Pennecke J, Brockbank KG, Fritze O, Schleicher M, *et al.* 2010. The performance of ice-free cryopreserved heart valve allografts in an orthotopic pulmonary sheep model. Biomaterials 20:5306–5311.

Liu Q, Wang H, Liu J, Huang H. 2010. AFM image processing for estimating the number and volume of nanoparticles on a rough surface. Surf Interface Anal 43:1354–1359.

Meiners S, Ahmed I, Ponery AS, Amor N, Harris SL, *et al.* 2007. Engineering electrospun nanofibers spinal cord repair: a discussion. Polymer Int 56:1340–1348.

Meiners S, Harris SL, Delgado-Rivera R, Ahmed I, Babu AN, *et al.* 2009. A nanofibrillar prosthetic modified with fibroblast growth factor-2 for spinal cord repair In; Chang WN. editor. Nanofibers: Fabrication, Performance, and Applications. Hauppage, NY: Nova Science Publishers, Inc, p 327–343.

Osher SJ, Rudin LI. 1990. Feature-oriented image enhancement using shock filters. SIAM J Numer Anal 27:919-940.

Schindler M, Ahmed A, Nur-E-Kamal A, Kamal J, Grafe TH, Chung HY, *et al.* 2005. Synthetic nanofibrillar matrix promotes in vivo-like organization and morphogenesis for cells in culture. Biomaterials 26:5624–5631.

Sitterberg J, Ozcetin A, Ehrhardt C, Bakowsky U. 2010. Utilising atomic force microscopy for the characterisation of nanoscale drug delivery systems. Eur J Pharm Biopharm 74:2–13.

Tiryaki VM, Ayres VM, Khan A, Delgado-Rivera R, Ahmed I, *et al.* 2010. Quantitative investigations of nanoscale elasticity of nanofibrillar matrices. Polymer nanofibers-fundamental studies and emerging applications. Mater Res Soc Symp Proc 1240E, Warrendale, PA.

Tiryaki VM, Ayres VM, Khan AA, Flowers DA, Ahmed I, *et al.* 2011. Investigation of nanofibrillar influence on cell-cell interactions of astrocytes by atomic force microscopies. Nanofunctional materials, nanostructures, and nanodevices for biomedical applications II. Mater Res Soc Symp Proc 1316E, Cambridge, UK.

Wang CC, Tsong TY, Hsu YH, Marszalek PE. 2011. Inhibitor binding increases the mechanical stability of staphylococcal nuclease. Biophys J 100:1094–1099.

Zhou M, Smith AM, Das AK, Hodson NW, Collins RW, *et al.* 2009. Self-assembled peptide-based hydrogels as scaffolds for anchorage-dependent cells. Biomaterials 30:2523–2530.

Zou Z, Zheng Q, Wu Y, Guo X, Yang S, Li J, *et al.* 2010. Biocompatibility and bioactivity of designer self-assembling nanofiber scaffold containing FGL motif for rat dorsal root ganglion neurons. J Biomed Mater Res A 95:1125–1131.